Journal of
Manufacturing and Materials Processing

MDPI

Article

On the Processing of a Powder Metallurgy Low-Cost Ti Alloy via Different Induction Sintering Strategies

Leandro Bolzoni [1,*], Valentin Roduit [1,2], Efrain Carreno-Morelli [2], Fei Yang [1] and Stella Raynova [1]

[1] School of Engineering, The University of Waikato, Hamilton 3240, New Zealand
[2] School of Engineering, University of Applied Sciences and Arts Western Switzerland, 1950 Sion, Switzerland
* Correspondence: leandro-bolzoni@waikato.ac.nz

Abstract

Reducing the cost of Ti alloys, both from a processing and compositional point of view, is a pathway forward for harnessing more extensively the industrial and environmental benefits associated with their uses, and it is an outstanding manufacturing challenge. Thus, this study investigated the manufacturing of a low-cost Ti alloy using different induction sintering strategies where both aspects are designed to reduce the final cost. The primary conclusion is that induction sintering of Ti alloys by cycling the temperature above and below the allotropic phase transformation (i.e., beta transus) suffices for the need for high green density values, which are commonly achieved using more expensive methods. This is due to faster densification kinetics. The fast uniform heating of the alloys leads to homogenous pore distribution in the entire volume and the dissolution of the alloying elements, especially during cycling sintering due to the fine particle size of the alloying elements. Consequently, despite the low homologous sintering temperatures used, the induction sintered low-cost Ti alloys do not fail catastrophically, although the ability to sustain plastic deformation is affected by the features of the residual porosity.

Keywords: titanium alloys; powder metallurgy; blended elemental; homogeneous microstructure; mechanical properties

1. Introduction

The combination of properties that make Ti alloys the ideal material for a broad range of engineering applications, spanning from aircraft components to biomedical devices and parts of pumps operating in highly corrosive environments, has been widely reported. This includes low density, high mechanical properties, corrosion resistance, and biocompatibility [1,2]. The main limitations that confine Ti alloys to high-demand applications [3,4] are primarily related to the high affinity for oxygen and poor machinability. They lead to a significantly higher cost per kilogram compared to competitor metals like steel [5] and Al [6]. Ti alloys are classified as α, α + β, and β depending on their microstructure. α alloys are known for better creep and corrosion resistance, β for enhanced formability and low stiffness, and α + β for the best compromise between strength and toughness. Additionally, the performance of α + β alloys, which are composed of two coexisting phases with different intrinsic responses can easily be tailored and adjusted by means of thermomechanical and heat treatments. Both alloys and treatments can lead to fully lamellar, fully equiaxed, or bimodal biphasic microstructures. This is without the need for chemical modifications and, hence, allows a broad range of properties to be achieved [7,8].

Check for updates

Academic Editor: Yogesh Kumar

Received: 25 August 2026
Revised: 16 September 2026
Accepted: 20 September 2026
Published: 22 September 2026

Copyright: © 2026 by the authors. Licensee MDPI, Basel, Switzerland. This article is an open access article distributed under the terms and conditions of the Creative Commons Attribution (CC BY) license.

Cast and wrought α + β alloys were developed using elements (e.g., V) that stabilize the beta phase and characterized by high solubility in both phases. These are, thus, known as isomorphous beta stabilizers. This was doned to avoid segregation and the precipitation of brittle intermetallic phases upon conventional processing (i.e., casting). However, most of these isomorphous beta stabilizers are intrinsically more expensive than Ti itself, exacerbating the cost issue. For a variety of reasons, but with cost reduction being the major driver, substitution of isomorphous beta stabilizers with eutectoid beta stabilizers is being investigated. This is particularly the case when alternative manufacturing methods such as powder metallurgy are used [9,10]. This is because the majority of these methods can completely circumvent the segregation and precipitation issues. The addition of Fe, which is one of the two eutectoid beta stabilizer elements with the highest beta stabilization power [11,12], is consequently considered very promising to develop the so-called low-cost Ti alloys. This is because Fe is a commodity metal and has high diffusivity in Ti [13,14].

To harness the advantages of powder metallurgy, which include overall lower energy demand (i.e., environmentally friendly), reduced reactivity, and prevention of brittle intermetallic precipitation, Ti alloys are commonly processed by vacuum sintering. This entails pressing the starting loose powders into the desired shape and consolidating the alloy at high temperature with a heat treatment (i.e., sintering) under high vacuum levels. For instance, Estaban et al. [15] analyzed the concurrent effect that Fe content and its particle size have on the mechanical behavior of Ti-(1-7)Fe alloys vacuum sintered in the 1100–1300 °C temperature range. Chen et al. [16] quantified the properties of binary Ti-(3-7)Fe alloys fabricated via cold press and vacuum sintering at 1250 °C subjected to different cooling conditions.

The combined addition of Fe and Al, to create the wrought-equivalent Ti-5Al-2.5Fe alloy via vacuum sintering (i.e., 700–1400 °C), has been analyzed by Siqueira et al. [17]. This is because Al is also a commodity metal and can help reduce cost and density, and enhance mechanical properties. The major disadvantage of vacuum sintering is, however, that it commonly requires processing cycles (i.e., create vacuum, heating, sintering, cooling, and break vacuum) in the range of 12–24 h. This is dependent on the size of the furnace and the achievable heating/cooling rate, which is generally around 5–10 °C/min. Consequently, we previously explored the possibility of using induction sintering to consolidate Ti alloys [18]. We demonstrated the feasibility of this manufacturing technique to significantly reduce the processing time due to its characteristic much faster heating rate [19–21]. Based on literature indicating that the driving force for sintering is increased when two phases coexist due to vacancies in concentration gradients [22], which enhances densification [23], we pioneered the use of cyclic induction sintering for the consolidation of the Ti-5Fe alloy [18]. Despite these advantages, cyclic sintering has not been properly explored, especially when using induction heating. Rare studies have been performed in the literature using electric resistance heating of WC-10Co cemented carbides [24] and spark plasma sintering of AlCoCrFeNi alloys [25].

This study, hence, aims at analyzing the differences in outcome when using (cyclic) induction sintering to manufacture the blended elemental low-cost Ti-2Al-3Fe alloy. The scope is to clarify the relationships between the resultant microstructure (i.e., phases, porosity, and chemical homogeneity) and associated mechanical and failure behavior. In particular, this study was designed to assess whether cyclic induction sintering can compensate for the need to have a high green density value, which generally requires a more complex process like warm pressing, to achieve comparable densification levels and mechanical properties.

2. Materials and Methods

The low-cost Ti alloy was produced by means of the blended elemental approach using commercial powders, whose characteristics are shown in Table 1. It can be seen that the selected alloying elements have smaller particle sizes and different morphologies with respect to the Ti powder. This aims at maximizing the sintering driving force, which is proportional to the particle size or associated surface energy, and the green density by using smaller powder particles able to fit in between the gaps left by the bigger Ti particles.

Table 1. Features of the starting powder per suppliers' specifications.

Element	Morphology	Max Particle Size	Purity	Oxygen Content	Supplier
Ti	Irregular	75 µm	>99.4%	0.25 wt.%	GoodFellow, Huntingdon, UK
Al	Spherical	45 µm	>99.5%	0.23 wt.%	GoodFellow, Huntingdon, UK
Fe	Spherical	10 µm	>99.7%	0.32 wt.%	ECKA Granules, Bell Bay, Australia

The desired amount of each starting powder was weighted, and 100 g homogeneous mixtures of the low-cost Ti alloy were obtained by blending the powders in a blender with V shape (Jiangyin Rongde Machinery, Wuxi, China) operated at 60 rpm for 30 min. The powder blends were subsequently shaped into 40 mm diameter cylindrical samples applying a uniaxial pressure of 600 MPa, resulting in a height of approximately 20 mm. As this study aims at investigating whether cyclic induction sintering with an approximate heating rate of 3.8 °C/s can suffice for the need for high values of green density, some samples were cold pressed (i.e., the ones to be cyclic induction sintered) and others were warm pressed (i.e., standard heat and hold induction sintering) as per Table 2. Specifically, two temperatures (i.e., 800 °C and 900 °C) with a constant holding time of 5 min were investigated for the standard heat and hold induction sintering route, and 4 cycles between 850 °C and 950 °C (i.e., across the beta transus of the alloy) was used for cyclic induction sintering.

Table 2. Details of the manufacturing parameters used.

Shaping	Sintering	Sintering Parameters	Shaping	Total Time
Warm pressing at 200 °C	Heat and hold	Initial heating to 800 °C, hold for 5 min	Warm pressing at 200 °C	~12 min
Warm pressing at 200 °C	Heat and hold	Initial heating to 900 °C, hold for 5 min	Warm pressing at 200 °C	~12 min
Cold pressing at 25 °C	Cyclic	Initial heating to 950 °C, 4 cycles between 850 °C and 950 °C	Cold pressing at 25 °C	~16 min

It is worth mentioning that the beta transus of the alloy used is approximately 886 °C, as estimated by means of the theoretical molecular orbital framework proposed by Morinaga et al. [26]. For sintering where the temperature is cycled across the beta transus of the alloy, diffusion across the interface, the strain linked to the presence of two coexisting phases, and the dislocations generated during the allotropic phase transformation between the alpha and beta Ti phases enhance the densification process [27,28]. Details of the in-house-made induction sintering experimental setup and typical heating rate (i.e., in the range of 3.8 °C/s) are available elsewhere [18]. However, it is worth mentioning that the equipment operates under purging Ar, guaranteeing an oxygen level below 200 ppm, and the samples were naturally cooled by turning off the induction heating unit.

Sintered samples were metallographically prepared using standard grinding with emery SiC papers plus polishing with OPS solution in order to analyze the distribution of the residual porosity left by the sintering process. Identification of the average and maximum pore size, as well as of the pore size distribution (i.e., frequency and accumulation) and the roundness of the pores, was performed by means of image analysis. For that, the ImageJ 1.54 open-source software, considering a minimum of 15 images across the whole volume of the sintered samples taken using an Olympus BX53M optical microscope (Olympus, Tokyo, Japan), was used. An average number of 300 pores was detected in each image, for a total of ~4500, whose overall size distribution was analyzed using the Feret diameter.

The metallographic samples were subsequently chemically etched for approximately 5 s using a water-based solution bearing 2% of HF and 6% of HNO_3 (i.e., Kroll reactant). Confirmation of the phases present in the sintered alloys was achieved through both optical micrographs and XRD analysis. A Philips X'Pert diffractometer (Philips, Amsterdam, The Netherland) with monochromatic Cu-K_α radiation (steep size of 0.013°, dwell time 1 s) was used for the latter. Further details of the microstructure and chemistry of the sintered alloys were attained by analyzing them by means of a Hitachi Regulus 8230 SEM (Hitachi, Ltd., Tokyo, Japan), which was also used for fractographic analysis.

The density of the pressed samples was quantified by dividing the mass and the volume of the samples. Triplicate measurements of the dimensions were obtained by means of a 2-decimal digital caliper. The density of the sintered samples was measured via the water displacement methodology, where the samples are weighted in air and under distilled water (i.e., Archimedes method). Relative values of the density were computed by dividing the measured density by the theoretical density of the alloy (i.e., 4.57 g/cm^3), as calculated by means of the rule of mixture from the density of the raw powders. The amount of porosity is the difference between the relative density values of the sintered samples and that of a fully dense alloy. The density change is the difference between the value of the relative density of the pressed and sintered samples, while the densification identifies the effectiveness of the sintering process.

Quantification of the mechanical behavior included hardness (N/mm^2) and tensile properties (i.e., yield stress, ultimate tensile strength, and strain) as measured on a minimum of three dog-bone samples (Figure 1) by means of an Instron 33R-4204 tester (Instron, Norwood, MA, USA). A crosshead speed of 0.1 mm/min while recording the elongation through an external mechanical extensometer was used. As the tensile samples were originally cut by means of electro discharge machining, their surfaces were ground with emery SiC papers to remove the oxide layer generated by the cutting process.

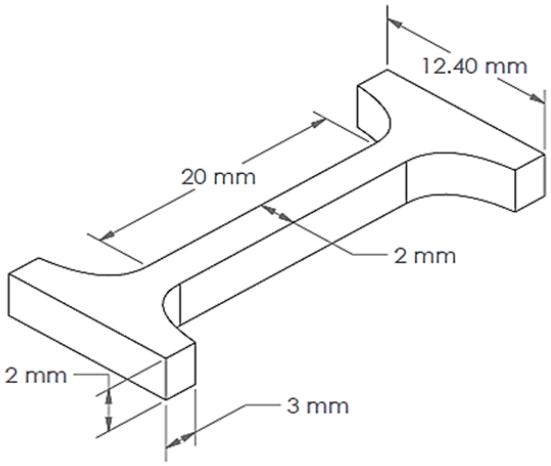


Figure 1. Sketch of the tensile samples used.

3. Results and Discussion

Representative optical micrographs of the induction sintered low-cost Ti alloys showing the distribution of the porosity are presented in Figure 2. It can be seen that, regardless of the sintering conditions, a homogenous distribution of pores is present. No major differences are clearly visible, as the amount of pores and their sizes seem to be comparable amongst the different conditions. This is confirmed by the measured average (i.e., 14.3 ± 0.8 µm) and maximum (i.e., 147.7 ± 8 µm) pore size, whose results are displayed in Figure 2d. However, a somewhat greater difference exists in terms of maximum pore size, as it is slightly higher for the low-cost Ti alloy sintered at 900 °C and slightly lower for the alloy sintered by cycling the temperature across the beta transus (i.e., 850–950 °C—4) in comparison to the alloy sintered at 800 °C. The achievement of a homogenous distribution of pores indicates that the samples were evenly heated up throughout their volume during induction sintering regardless of the actual sintering cycle used. Induction sintering is characterized by a very high heating rate and short dwell time (i.e., ~15 min) in comparison to vacuum sintering (i.e., 12–24 h); therefore, the achievement of a consistent heating of the samples is technologically significant.

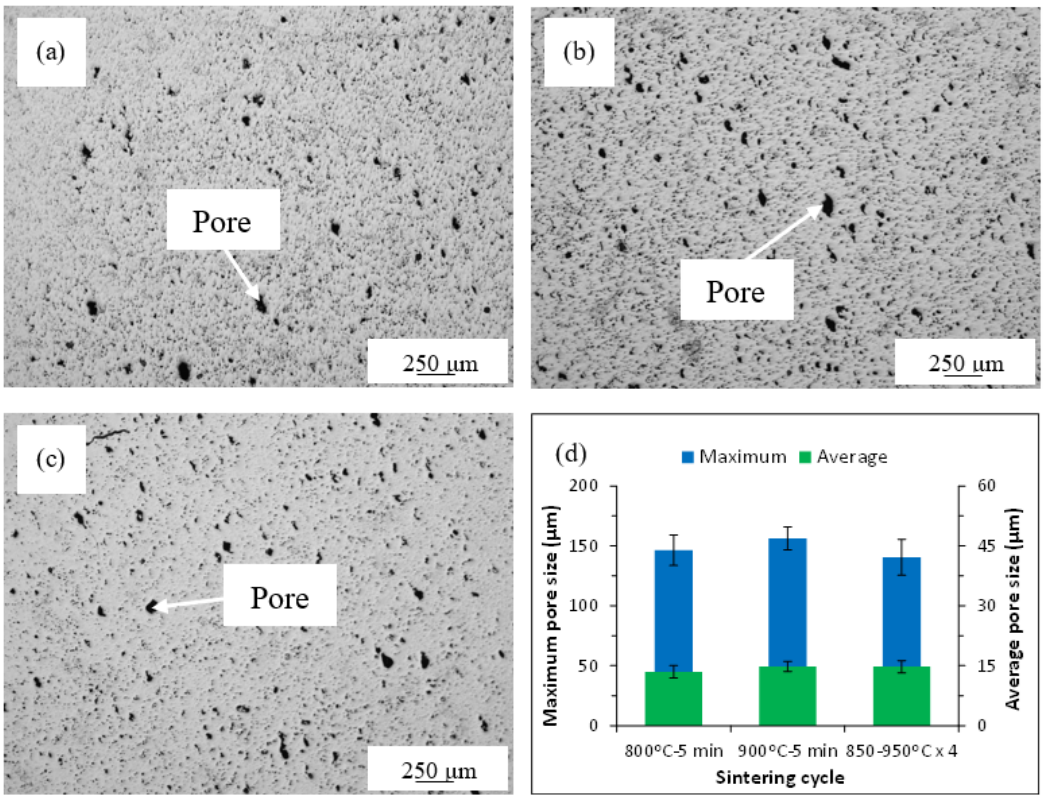


Figure 2. Optical micrographs of the induction sintered low-cost Ti alloys showing the distribution of the porosity: (**a**) 800 °C-5 min, (**b**) 900 °C-5 min, and (**c**) 850–50 °C—4 cycles, and (**d**) maximum and average pore sizes.

Figure 3 shows a more in-depth analysis of the features of the residual porosity as frequency and cumulative distribution of both the pore size and the roundness of the pores. It can be seen that the induction sintered low-cost Ti alloys are characterized by a normal distribution of pores centered around 9–15 µm, regardless of the sintering cycle. However, the actual amount of pores with 9–15 µm size decreases from using 800 °C-5 min (i.e., 44.8%) to 850–950 °C—4 cycles (i.e., 37.0%) as a consequence of the higher sintering temperature, which is expected to result in a higher densification. In terms of cumulative behavior, the alloys display a sigmoidal curve, with more than 70% of the pores having a size lower than

15 µm. It is worth mentioning that, despite reaching a maximum pore size around 150 µm, only a very small fraction of pores is actually bigger than 30 µm. Specifically, 4.8%, 7.8%, and 8.1% are respectively found to have a size > 30 µm for the low-cost Ti alloys induction sintered through 800 °C-5 min, 900 °C-5 min, and 850–950 °C—4 cycles. The presence of a greater amount of bigger pores is, once again, related to the specific sintering conditions.

The analysis of the roundness of the pores shows that the induction sintered low-cost Ti alloys are characterized by an exponentially decreasing frequency trend or, in turns, an asymptotically increasing cumulative trend [29]. It can be seen that the total amount of pores with spherical morphology increases from 800 °C-5 min (i.e., 43.1%) to 850–950 °C—4 cycles (i.e., 58.0%), and it is much more similar between the latter and 900 °C-5 min (i.e., 56.4%). This is because the sintering temperature of 900 °C is meant to be above the beta transus and diffusion is faster in the b.c.c. beta titanium phase with respect to the h.c.p. alpha titanium phase, and so is mainly cycling in the 850–950 °C temperature range.

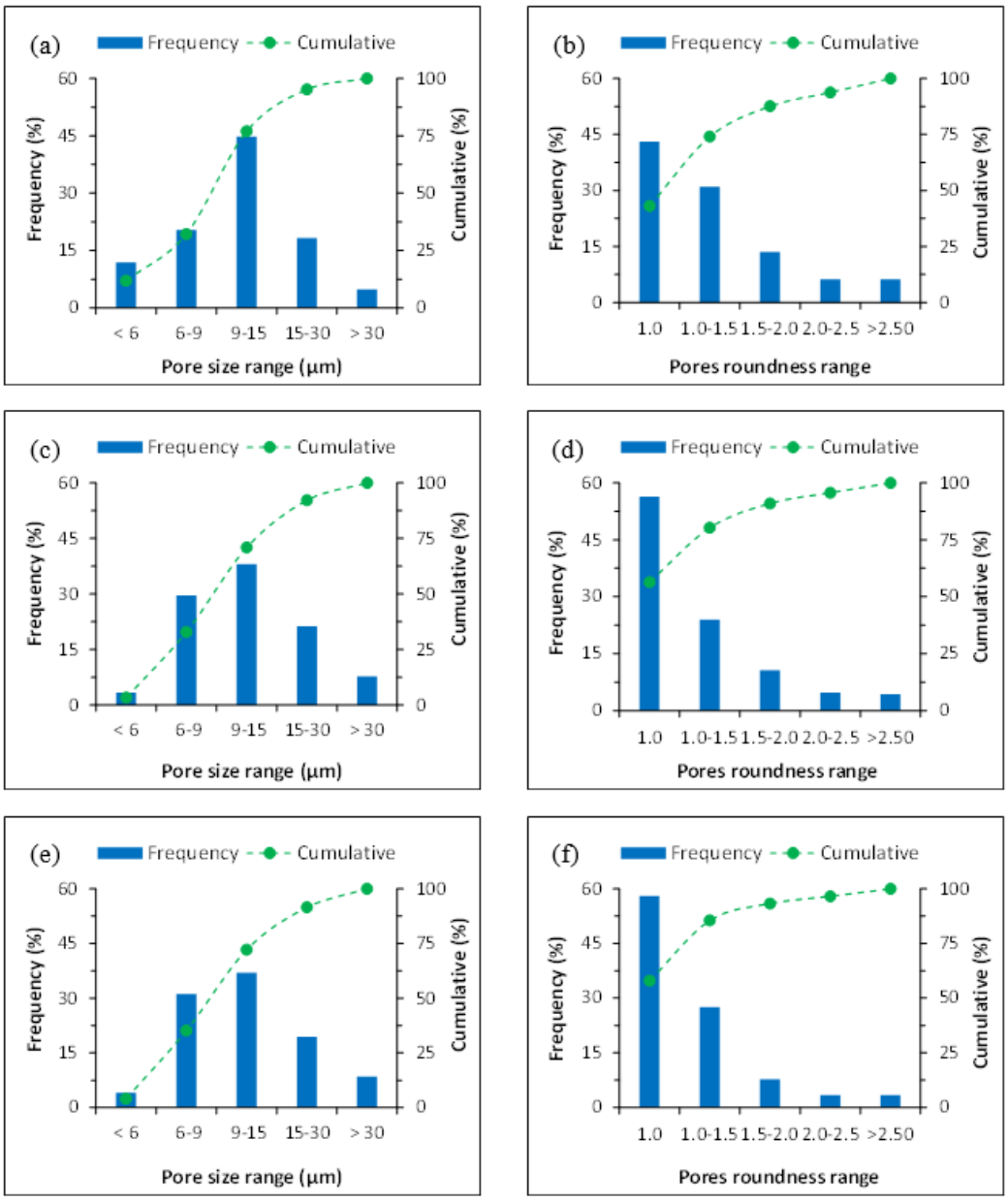


Figure 3. Frequency and cumulative distribution of the pore size and roundness, respectively, of the induction sintered low-cost Ti alloys: (**a**,**b**) 800 °C-5 min, (**c**,**d**) 900 °C-5 min, and (**e**,**f**) 850–950 °C—4 cycles.

Congruently, the overall number of highly irregular pores decreases, as the number of pores with a roundness value greater than two is 12.4%, 9.0%, and 6.8% for the low-cost Ti alloys induction sintered using, respectively, 800 °C-5 min, 900 °C-5 min, and 850–950 °C—4 cycles. As per the classical sintering theory, the rounding of pores and the associated formation of close pores is typical of the intermediate stage of sintering. This is expected when reaching relative density values around 90–92% [30–32].

Optical micrographs showing the overall distribution of the phases present in the induction sintered low-cost Ti alloys are shown in Figure 4. It can be seen that the alloys display the typical lamellar microstructure of α + β titanium alloys [33,34]. Such microstructure is constituted by equiaxed alpha grains, which initially transform from the prior beta grains upon crossing the beta transus temperature during cooling.

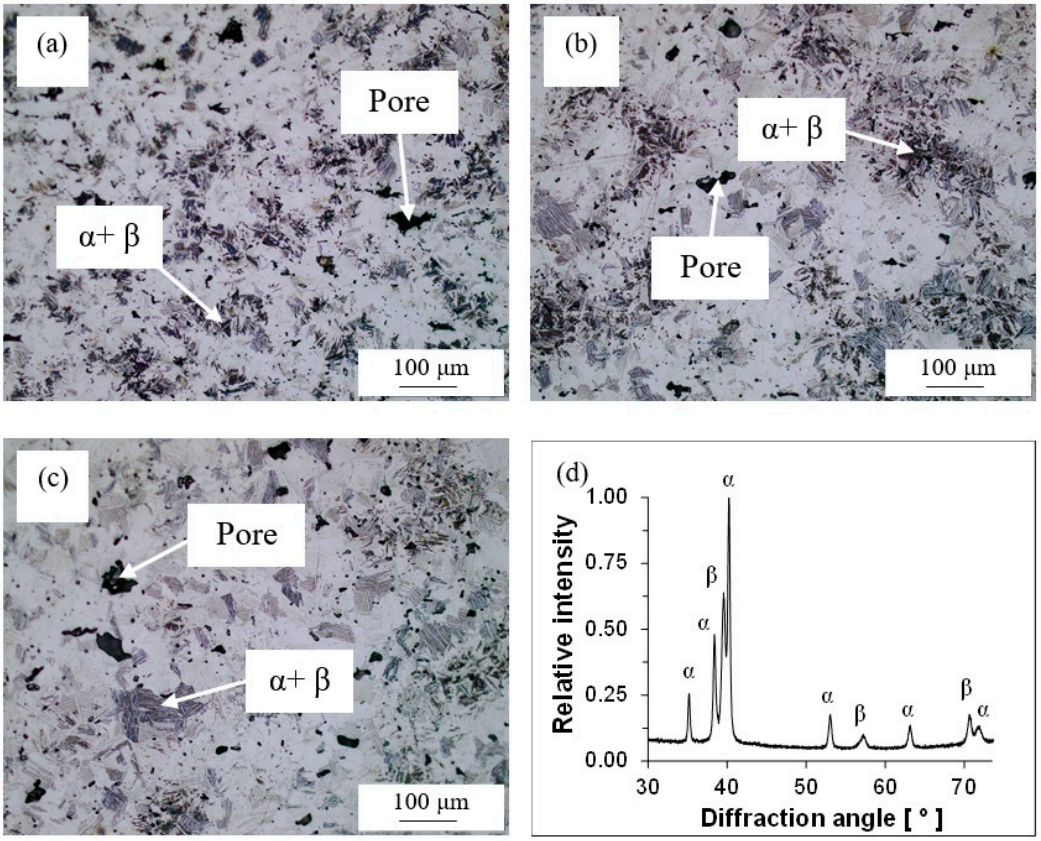


Figure 4. Representative optical micrographs of the induction sintered low-cost Ti alloys showing the grain structure: (**a**) 800 °C-5 min, (**b**) 900 °C-5 min, and (**c**) 850–950 °C—4 cycles, and (**d**) representative XRD pattern.

It can be noticed that the size of these alpha grains is comparable to that of the starting titanium powder particles (i.e., maximum size < 75 µm as per Table 1). This is due to the short sintering cycle enabled by induction heating. Due to the presence of iron as beta stabilizer, alternating parallel alpha and beta lamellae nucleate at the prior beta grain boundaries and are therefore found within the equiaxed alpha grain. No clear signs of undissolved alloying elements powder particles are visible, suggesting a fairly homogenous chemistry. This is confirmed by the absence of XRD peaks relative to the elemental aluminum and iron powders as per the representative XRD pattern of Figure 4d. Exclusively peaks of the stable alpha and beta titanium phases were detected, resulting in an average volume fraction of, respectively, 70.6 ± 0.8% and 29.4 ± 0.5%. From this it is also inferred that no precipitated intermetallic phases, like Ti–Fe that might be expected on the basis of the equilibrium Ti–Fe phase diagram [35], or transient intermetallic phases are

present. The latter have previously been detected during sintering of titanium alloys and disappear as dissolution of the alloying elements powder particles progresses [36].

Figure 5 shows high-magnification SEM micrographs of the induction sintered low-cost Ti alloys, confirming the presence of alpha + beta lamellae enclosed in alpha grain boundaries. The size of the features of the lamellar microstructure is comparable between the different induction sintered low-cost Ti alloys, and so is, roughly, their volume fraction. Despite not being clearly identifiable via optical microscopy, SEM analysis shows that a few areas with incomplete dissolved iron particles are present in the low-cost Ti alloys induction sintered at 800 °C-5 min (Figure 5d), while no aluminum powder particles were found. This is because aluminum dissolved readily in titanium, leaving behind Kirkendall porosity, due to its very high diffusivity in both the alpha and beta titanium phases [37]. Additionally, the diffusivity of aluminum in titanium is faster than the other way around (i.e., titanium diffusing into aluminum), as reported in the literature [36,38].

Similarly, iron has high diffusivity in titanium, but due to its higher melting point, the driving force for its dissolution is comparatively lower. For instance, 800 °C is approximately 0.6 of its absolute melting point. Consequently, despite the smaller particle size of the iron powder particles in comparison to aluminum (Table 1), some of the iron powder particles with the greatest size do not reach complete dissolution. No areas with evident partially dissolved particles were found in the low-cost Ti alloys induction sintered at 900 °C-5 min (Figure 5e), indicating their complete dissolution. However, a few highly localized areas close to the biggest, mainly irregular, pores do not reach a complete homogenization of the alloying elements, indicating that those are Kirkendall pores.

In the case of the alloy induction sintered by cycling the temperature across the beta transus, complete dissolution of the alloying elements powder particles is achieved along with the full homogenization of the chemistry, per EDS chemical analysis (Figure 5f). Thus, obtaining a fully homogeneous distribution of the alloying elements at low temperature, as higher homologous sintering temperatures are generally needed when sintering blended elemental titanium alloys [39–41], is technologically significant. This is related to the enhanced densification expected as a result of faster diffusion attributed to interface diffusion [28] due to the coexistence of two phases around the beta transus. In particular, diffusion of the alloying elements starts upon the first heating cycle at the alpha grain boundaries of the titanium powder particles. This leads to the stabilization of some beta phase due to the dissolution of iron. During the first cooling, some stabilized beta reverts back to alpha. This creates interphase interfaces with the associated mismatch strain and formation of dislocations, where these defects enhance the overall diffusion of the sintering process [42]. The same is repeated in subsequent heating cycles, resulting in the homogenization of the chemical elements and a faster densification.

The values of the density of the pressed low-cost Ti alloys (i.e., green density) are shown in Figure 6, where it can be seen that for both 800 °C-5 min and 900 °C-5 min, there is only a marginal difference between them, while the difference is significantly bigger in the case of 850–950 °C—4 cycles. Such difference in behavior is primarily due to the fact that the alloys sintered using 800 °C-5 min and 900 °C-5 min were warm pressed (Table 2), whereas the alloy to be sintered via cyclic induction sintering was cold pressed.

As previously discussed, this was purposely done in order to investigate whether induction sintering titanium alloys by cycling the temperature across their beta transus can compensate for the need to use warm pressing. This is because the latter is more labor and energy intensive, and it requires a more complex setup to reach high levels of relative density. It can be noticed that despite their difference in terms of green density, the three alloys reach a similar value of density after induction sintering regardless of the sintering cycle. Additionally, the values of the sintered density are lower in comparison to the

theoretical density value of the alloy. Coherently, the induction sintered low-cost Ti alloys have some residual porosity, in agreement with Figure 2, which is fairly comparable (i.e., 6.3 ± 0.5%) among the three alloys (Figure 6b). Moreover, it can be seen that the change in density, and the associated densification, increases with the sintering temperature, and they are significantly higher—respectively, 9.8% and 58.9% (Figure 6c)—when sintering the alloys by cycling the temperature across the beta transus. This is a direct consequence of the fact that the alloys sintered using 850–950 °C—4 cycles were cold pressed, but reinforces the finding that using cyclic sintering is beneficial to enhance the densification of Ti alloys.

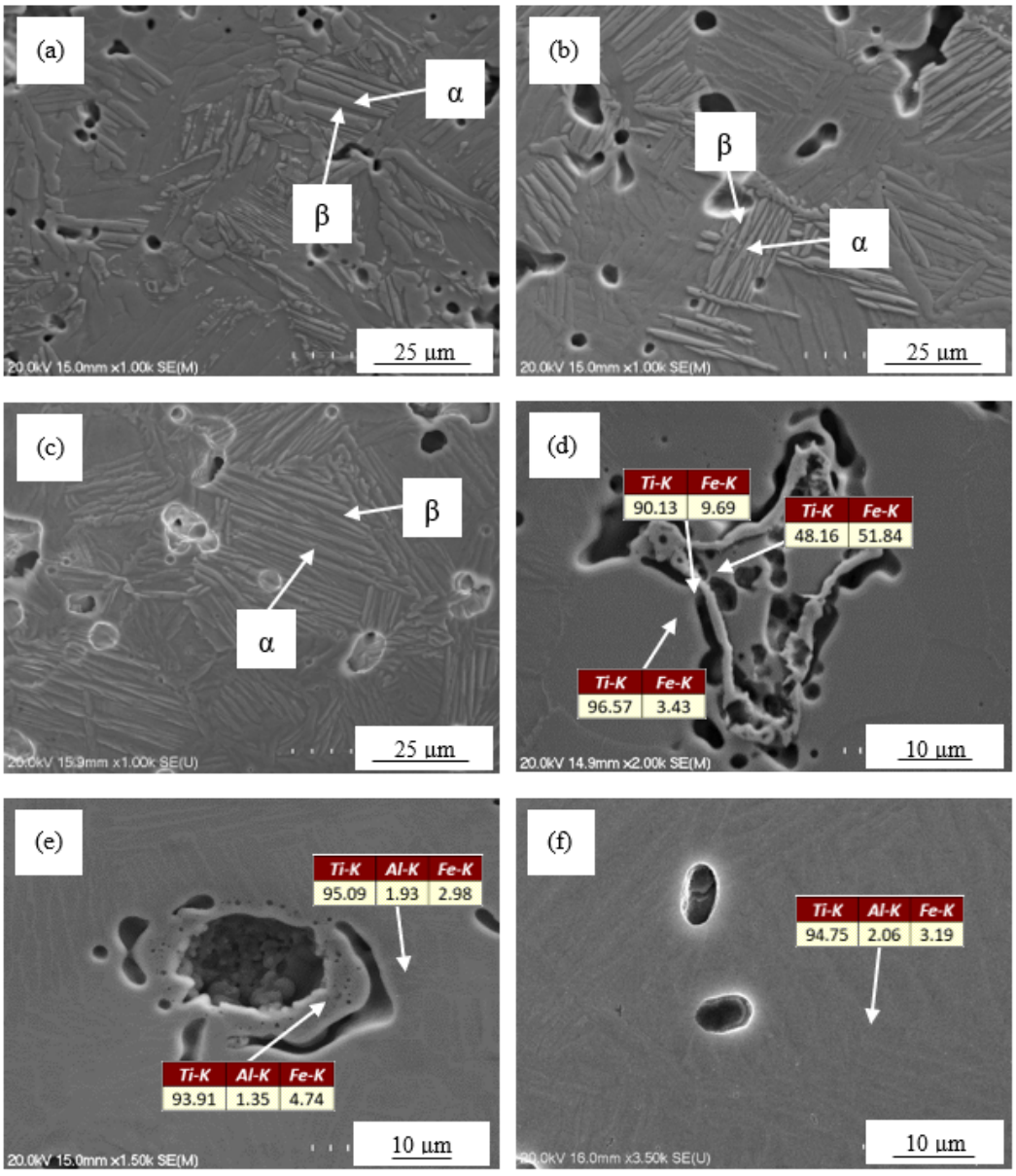


Figure 5. Representative SEM micrographs of the induction sintered low-cost Ti alloys showing the distribution of the phases: (**a**) 800 °C-5 min, (**b**) 900 °C-5 min, and (**c**) 850–950 °C—4 cycles, (**d**) micrograph showing a partially dissolved iron particle found after sintering at 800 °C-5 min, (**e**) micrograph showing a highly localized incomplete homogenization of the alloying elements after sintering at 900 °C-5 min, and (**f**) micrograph showing complete homogenization of the alloying elements after sintering at 850–950 °C—4 cycles. Note: compositions are in weight percentage (i.e., wt.%).

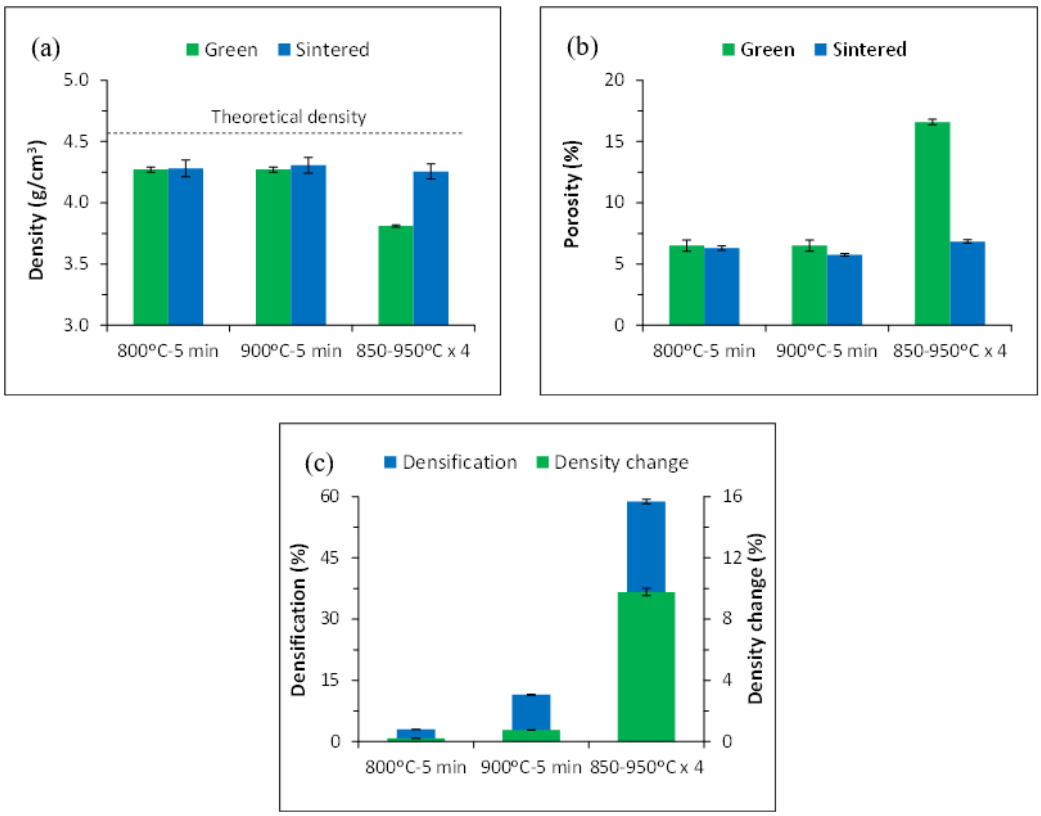


Figure 6. Variation of the physical properties of the induction sintered low-cost Ti alloys: (**a**) density, (**b**) porosity, and (**c**) densification and density change.

Figure 7 shows representative results of the mechanical behavior of the induction sintered low-cost Ti alloys. From the stress–strain curves (Figure 7a), it can be seen that the alloys are able to undergo some plastic deformation before failure, and they are characterized by comparable stiffness (i.e., 95 ± 2 GPa).

Coherently with the low plastic deformation ability, the fracture surface of the induction sintered low-cost Ti alloys is fairly rough. It has both areas with small dimples where plastic deformation happened and intergranularly failed zones that fractured in a more brittle way. There is also a large number of areas with smooth surfaces, especially in close proximity to the residual pores, where the alloys did not deform and led to the formation of tear ridges. This seems to indicate that the main mode of failure is intergranular facilitated by the presence of residual pores, which provide a preferential crack growth pathway (Figure 7b–d). An increase in the induction sintering temperature from 800 °C to 900 °C is beneficial to improve the mechanical properties, as higher-yield stress and strain values (Figure 7e), as well as ultimate tensile strength and hardness (Figure 7f), are obtained. This is primarily related to the slightly lower level of residual porosity and slightly higher densification (Figure 6) achieved. In the case of the titanium alloys induction sintered by cycling the temperature across their beta transus (i.e., 850–950 °C—4 cycles), the properties are more comparable to those of the alloy sintered at 900 °C-5 min. Precisely, the yield stress and hardness are slightly higher (i.e., 742 ± 16 MPa vs. 730 ± 17 MPa and 877 ± 3 N/mm^2 vs. 831 ± 4 877 ± 3 N/mm^2, respectively), and the strain and ultimate tensile strength slightly lower (i.e., 1.3 ± 0.1% vs. 1.6 ± 0.3% and 784 ± 28 MPa vs. 799 ± 4 MPa, respectively). It is worth mentioning that the achieved mechanical properties are also affected by the content of oxygen, which notoriously strengthens and embrittles titanium [43,44].

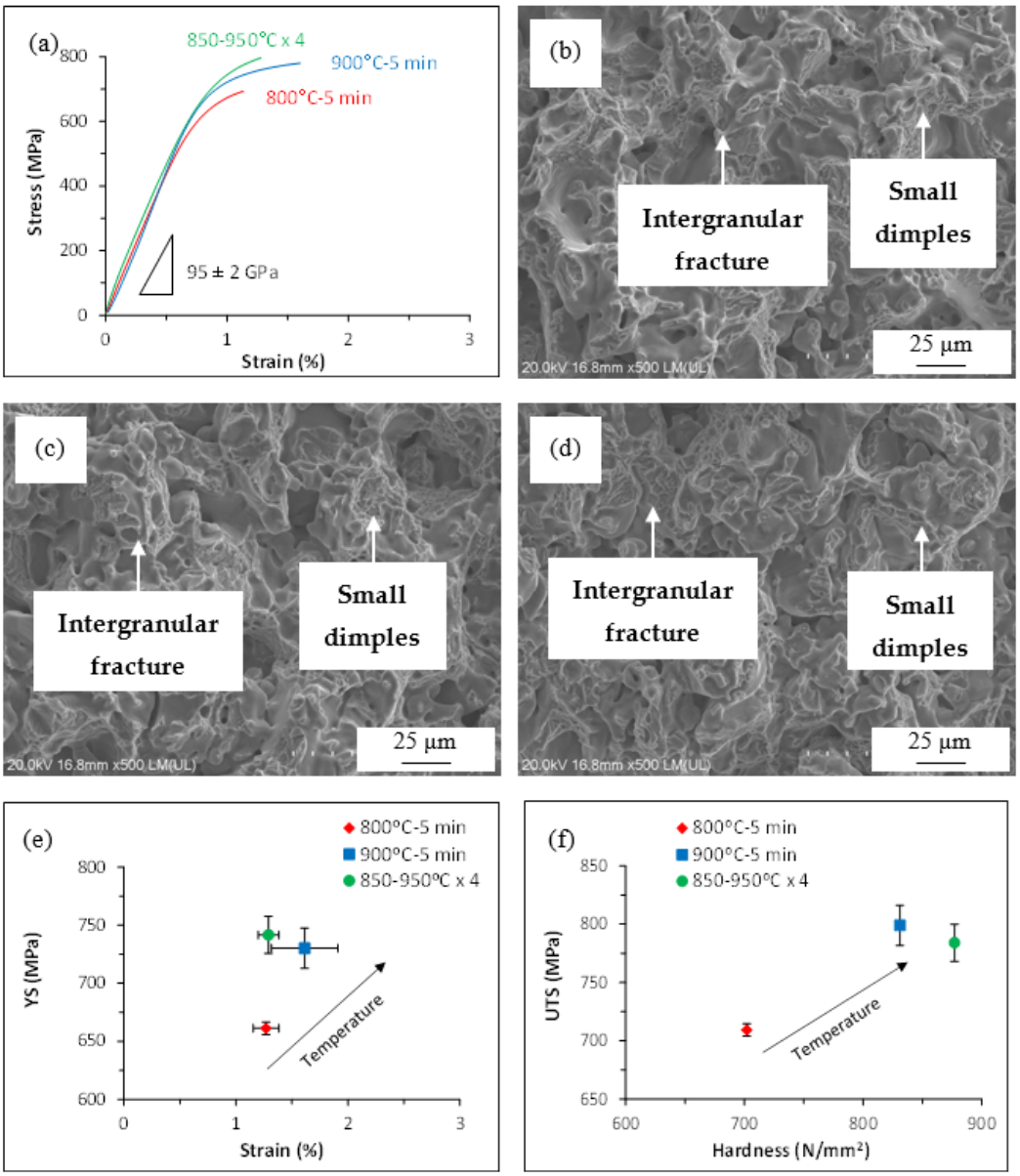


Figure 7. Representative results of the mechanical behavior of the induction sintered low-cost Ti alloys: (**a**) stress–strain curves, (**b**) 800 °C-5 min fractographic image, (**c**) 900 °C-5 min fractographic image, (**d**) 850–950 °C—4 cycles fractographic image, (**e**) yield stress versus strain, and (**f**) ultimate tensile strength versus hardness.

A correlation between the features of the microstructure of the induction sintered low-cost Ti alloys, which include aspects like residual porosity and densification, and their mechanical behavior is shown in Figure 8 by means of a linear regression heat map. It is found that the resistance to plastic deformation (i.e., YS, UTS, and hardness) depends on the average pore size but not the maximum size, the average pore roundness, and the average interlamellar spacing. This is because the microstructural features with size in the range of around a tenth of a micrometer have a more direct impact on the movement of dislocations [45,46].

It can be seen that a correlation exists among the mechanical responses, which is not the case when they are related to the elongation (i.e., strain). For the latter, the most important aspects, ordered in terms of a progressively lower impact, are maximum pore size, amount of porosity, and average pore roundness. The maximum dimension of the pores is critical, as they constitute stress concentration sites. The bigger the pore, the greater

the stress concentration, especially if it has a non-spherical morphology. Furthermore, the presence of a greater amount of pores can promote the establishment of a preferential pathway for crack growth, leading to a rough fractographic surface (Figure 7). From this analysis, it is also found that the amount of porosity is related to the maximum pore size, the average pore size, and the average pore roundness. This is in agreement with the results of the pore size distribution shown in Figure 3. Interestingly, in the case of the induction sintered low-cost Ti alloys of this study, the average interlamellar spacing correlates well with the average pore size and roundness. This is because they are all dependent on the local diffusion at grain boundaries upon the dissolution of the alloying elements prior to the cooling from the sintering temperature (Figure 5). The effect of the particle size of the alloying elements, which is taken into account by the densification of the alloy, is rather limited.

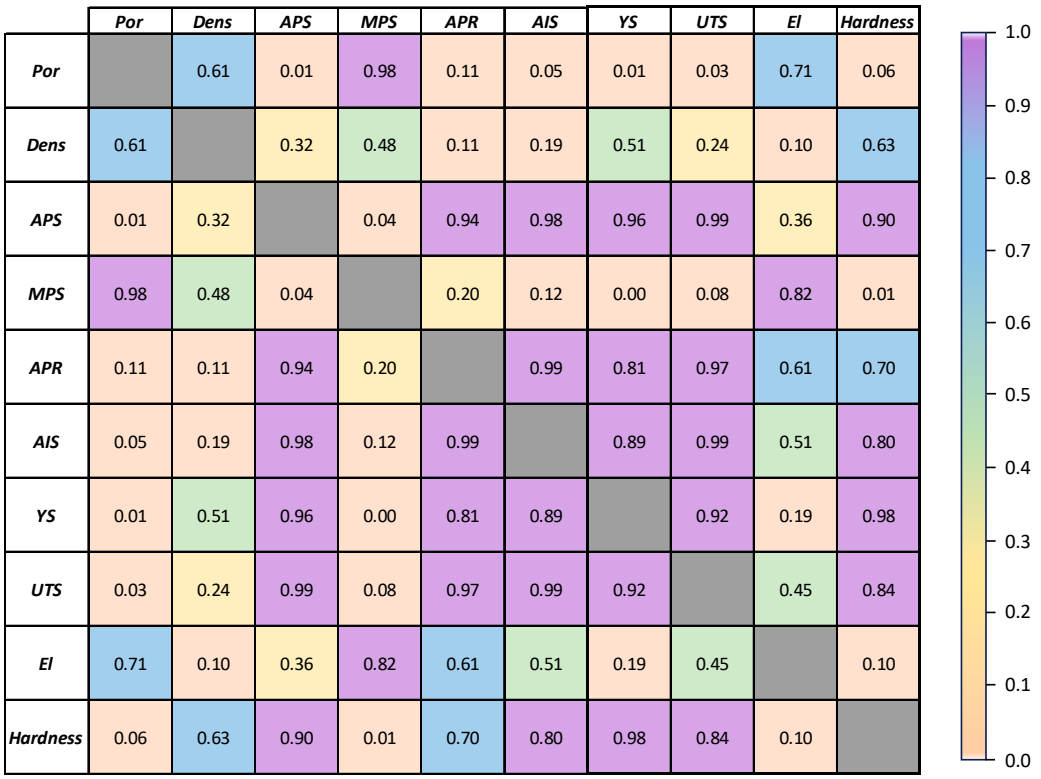


Figure 8. Linear regression heat map showing the correlation between the features of the microstructure of the induction sintered low-cost Ti alloys and their mechanical behavior. Legend: *Por*—amount of porosity, *Dens*—densification, *APS*—average pore size, *MPS*—maximum pore size, *APR*—average porosity roundness, *AIS*—average interlamellar spacing, *YS*—average yield stress, *UTS*—average ultimate tensile strength, and *El*—average elongation.

A comparison of the performance achieved in this study with those of other Ti alloys with similar amounts of alloying elements (e.g., Ti-3Al-2.5V) processed by means powder metallurgy methods is shown in Figure 9 in terms of relative density and mechanical behavior. The level of relative density is compared using the temperature-compensated time parameter (θ), as calculated using Equation (1) [34]. This takes into account the combined effect of the sintering conditions (i.e., heating rate, maximum temperature, and dwell time):

$$\theta = t \cdot exp^{\left(\frac{-Q}{RT}\right)} \quad (1)$$

where t is the sum of the heating and dwell sintering time, Q is the activation energy for self-diffusion in Ti (i.e., 194 kJ/mol [47]), R is the gas constant, and T is the absolute sintering temperature.

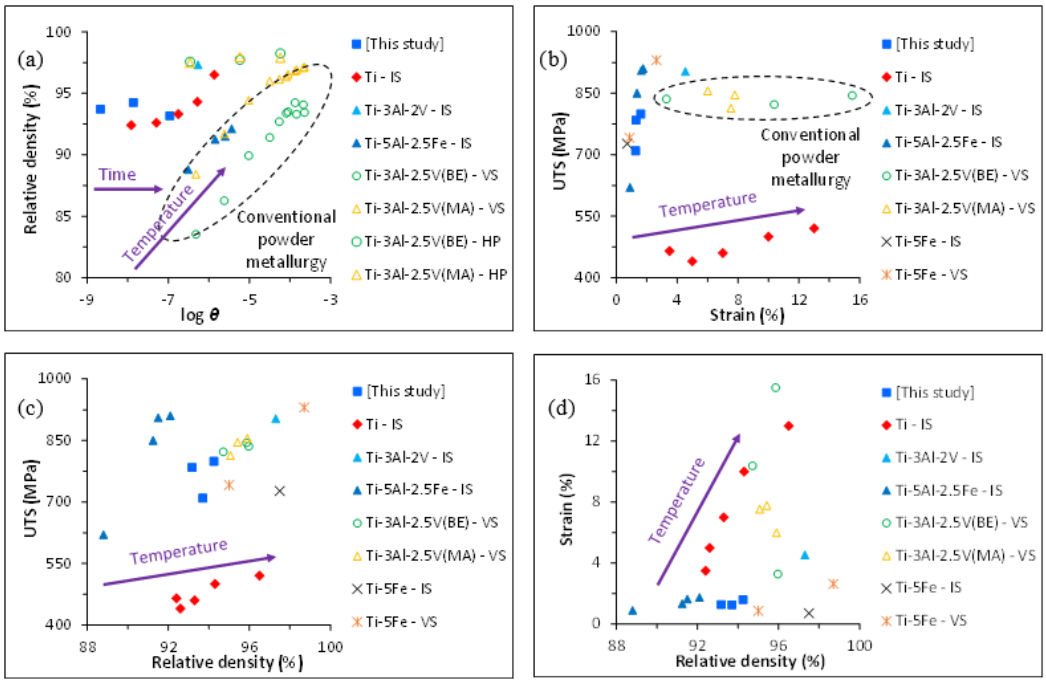


Figure 9. Comparison of the relative density (**a**) and mechanical behavior (**b**–**d**) of the induction sintered low-cost Ti alloys of this study with the literature. Legend: *IS*—induction sintering, *VS*—vacuum sintering, *BE*—blended elemental, *MA*—master alloy, and *HP*—hot pressing.

It is found that the induction sintered low-cost Ti alloys reach similar relative density levels to those of other Ti alloys but in a much shorter time. This is beneficial in terms of cost reduction and environmental impact. The introduction of an applied pressure during the sintering stage (i.e., *HP*) only increases the level of relative density marginally (Figure 9a). This makes the fast induction heating very competitive from a manufacturing point of view. The comparison of the UTS/strain pairs in Figure 9b shows that the induction sintered low-cost Ti alloys of this study reach comparable strength values to those of similar alloys, all of them being stronger than Ti. This is primarily due to the presence of the alloying elements and the associated strengthening mechanisms (i.e., solid solution, stabilization of the beta phase, and refinement of the microstructure). However, it can also be seen that the amount of plastic deformation sustained before non-catastrophic failure is comparatively lower with respect to Ti alloys processed by means of the conventional powder metallurgy route for Ti (i.e., vacuum sintering) and compared to induction sintered Ti. This is primarily due to the specific sintering temperature used in each instance and the related microstructural changes, which are summarized in potentially higher levels of relative density and grain growth. Both a lower amount of pores—especially if they have an irregular morphology, which has a higher stress concentration factor—and coarser grains favor ductility.

The analysis of the UTS values against the relative density level (Figure 9c) shows that, in reality, the induction sintered low-cost Ti alloys of this study have strength values similar to or greater than other alloys, despite their slightly lower relative density level, though the actual level of relative density is not so critical starting from 90%. Consequently, there is still a very clear influence from the actual chemistry of the alloy, as each alloying element stabilizes one phase (either alpha or beta). Each alloying element has a different intrinsic stabilization power, which is commonly taken into account by means of the molybdenum

equivalent parameter [11,12]. In the case of the strain versus relative density (Figure 9d), it is found that the values of the induction sintered low-cost Ti alloys sit at the bottom of the range of values achieved, though some of the other induction sintered alloys have higher relative density values. Once again, there is a clear effect from the composition, as well as from the sintering parameters. Therefore, the level of relative density has a significantly greater impact on the achievable strain with respect to the effect on the strength (Figure 8).

4. Conclusions

This study analyzed the processing of a low-cost Ti alloy via different induction sintering strategies entailing either heating up to the sintering temperature plus holding the alloy at the temperature or sintering by cycling the temperature above and below the allotropic phase transformation repeatedly four times. As one of the aims was to clarify whether cyclic sintering circumvents the need for high green density values, samples were, respectively, either warm or cold pressed. The resulting microstructural features (i.e., phases, porosity, and chemical homogeneity) were thus quantified and related to the mechanical response. The fast induction sintering process leads to the formation of microstructures with a homogenous distribution of residual pores with comparable average and maximum size. This confirms that induction sintering guarantees an even heating of the samples throughout their volume. Subtle differences exist in the distribution of the residual porosity as a function of the sintering cycle, which also affects the homogeneity of the distribution of the alloying elements. However, the alloys are always characterized by the expected lamellar microstructure of $\alpha + \beta$ titanium alloys without the presence of harmful precipitated intermetallic compounds. A complete dissolution of the alloying elements is guaranteed by cyclic induction sintering, supported by the use of alloying elements with fine particle size. This study shows that cyclic induction sintering enhances the densification kinetics, fully compensating for the starting lower green density. Moreover, it permits achieving similar sintered density values to more conventional powder metallurgy methods. Even though low homologous sintering temperatures were used, the induction sintered low-cost Ti alloys do not fail catastrophically, with the strength increasing with the sintering temperature. However, the amount of sustained plastic deformation is limited, primarily due to the presence of the residual pores. They act as a stress concentration site, resulting in a rough, primarily intergranular, fracture surface. From the correlation between the microstructural features and mechanical behavior, the resistance to plastic deformation depends on average pore size and roundness, as well as interlamellar spacing. Conversely, the ductility is mostly affected by maximum pore size, the amount of porosity, and average pore roundness. The induction sintered low-cost Ti alloys of this study reach similar relative sintered density and mechanical response to those of comparable Ti alloys obtained by means a variety of powder metallurgy methods, making it very competitive from a manufacturing point of view.

Author Contributions: Conceptualization, L.B. and S.R.; methodology, L.B., V.R., E.C.-M., F.Y., and S.R.; formal analysis, L.B., V.R., E.C.-M., F.Y., and S.R.; investigation, L.B., V.R., E.C.-M., F.Y., and S.R.; data curation, L.B., V.R., E.C.-M., F.Y., and S.R.; writing—review and editing, L.B.; supervision, L.B. and E.C.-M. All authors have read and agreed to the published version of the manuscript.

Funding: This research did not receive any specific grant from funding agencies in the public, commercial, or not-for-profit sectors.

Data Availability Statement: All metadata pertaining to this work will be made available on reasonable request.

Conflicts of Interest: The authors declare no conflicts of interest.

References

1. Qi, P.; Li, B.; Wang, T.; Zhou, L.; Nie, Z. Microstructure and Properties of a Novel Ternary Ti-6Zr-xFe Alloy for Biomedical Applications. *J. Alloys Compd.* **2021**, *854*, 157119. [CrossRef]
2. Yumak, N.; Aslantaş, K. A Review on Heat Treatment Efficiency in Metastable β Titanium Alloys: The Role of Treatment Process and Parameters. *J. Mater. Res. Technol.* **2020**, *9*, 15360–15380. [CrossRef]
3. Henriques, V.A.R.; de Campos, P.P.; Cairo, C.A.A.; Bressiani, J.C. Production of Titanium Alloys for Advanced Aerospace Systems by Powder Metallurgy. *Mater. Res.* **2005**, *8*, 443–446. [CrossRef]
4. Geetha, M.; Singh, A.K.; Asokamani, R.; Gogia, A.K. Ti Based Biomaterials, the Ultimate Choice for Orthopaedic Implants—A Review. *Prog. Mater. Sci.* **2009**, *54*, 397–425. [CrossRef]
5. García-Junceda, A.; Díaz-Rivera, C.; Gómez-Torralba, V.; Rincón, M.; Campos, M.; Torralba, J.M. Analysis of the Interface and Mechanical Properties of Field-assisted Sintered Duplex Stainless Steels. *Mater. Sci. Eng. A* **2019**, *740–741*, 410–419. [CrossRef]
6. Bolzoni, L.; Babu, N.H. Towards Industrial Al-Nb-B Master Alloys for Grain Refining Al-Si Alloys. *J. Mater. Res. Technol.* **2019**, *8*, 5631–5638. [CrossRef]
7. Luo, Y.; Xie, Y.; Zhang, Z.; Liang, J.; Zhang, D. Improving Strain Hardening Capacity of High-strength Ti-6Al-4V Alloy by a Dual Harmonic Structure. *J. Mater. Res. Technol.* **2023**, *26*, 1122–1135. [CrossRef]
8. Li, Y.; Zhang, Q.; Zhao, R.; Wang, H.; Liu, Y.; Zhao, Z.; Yang, C.; Zhang, L. Improved Strength and Corrosion Resistance of Ti-50Zr Alloy Through Heat Treatment. *Adv. Eng. Mater.* **2025**, *27*, e202501828. [CrossRef]
9. Klein, T.; Zhang, D.; Staufer, E.; Boll, T.; Schneider-Broeskamp, C.; Edtmaier, C.; Schmitz-Niederau, M.; Horky, J.; Qiu, D.; Easton, M. Phase Transformation Pathways in a Ti-5.9Cu Alloy Modified with Fe and Al. *J. Mater. Res. Technol.* **2023**, *27*, 4978–4985. [CrossRef]
10. Bolzoni, L.; Esteban, P.G.; Ruiz-Navas, E.M.; Gordo, E. Influence of Powder Characteristics on Sintering Behaviour and Properties of PM Ti Alloys Produced from Prealloyed Powder and Master Alloy. *Powder Metall.* **2011**, *54*, 543–550. [CrossRef]
11. Molchanova, K. *Phase Diagrams of Titanium Alloys*; Translation of Atlas Diagram Sostoyaniya Titanovyk Splavov; Israel Program for Scientific Translations: Jerusalem, Isreael, 1965; p. 154.
12. Bania, P.J. Beta Titanium Alloys and Their Role in the Titanium Industry. *JOM* **1994**, *46*, 16–19. [CrossRef]
13. Hidalgo, A.A.; Frykholm, R.; Ebel, T.; Pyczak, F. Powder Metallurgy Strategies to Improve Properties and Processing of Titanium Alloys: A Review. *Adv. Eng. Mater.* **2017**, *19*, 1600743. [CrossRef]
14. Umeda, J.; Tanaka, T.; Teramae, T.; Kariya, S.; Fujita, J.; Nishikawa, H.; Shibutani, Y.; Shen, J.; Kondoh, K. Microstructures Analysis and Quantitative Strengthening Evaluation of Powder Metallurgy Ti-Fe Binary Extruded Alloys with (α+β)-dual-phase. *Mater. Sci. Eng. A* **2021**, *803*, 140708. [CrossRef]
15. Esteban, P.G.; Ruiz-Navas, E.M.; Gordo, E. Influence of Fe Content and Particle Size on the Processing and Mechanical Properties of Low-cost Ti-xFe Alloys. *Mater. Sci. Eng. A* **2010**, *527*, 5664–5669. [CrossRef]
16. Chen, B.-Y.; Hwang, K.-S.; Ng, K.-L. Effect of Cooling Process on the Alpha Phase Formation and Mechanical Properties of Sintered Ti-Fe Alloys. *Mater. Sci. Eng. A* **2011**, *528*, 4556–4563. [CrossRef]
17. Siqueira, R.; Sandim, H.; Hayama, A.; Henriques, V. Microstructural Evolution during Sintering of the Blended Elemental Ti-5Al-2.5Fe Alloy. *J. Alloys Compd.* **2009**, *476*, 130–137. [CrossRef]
18. Bolzoni, L.; Roduit, V.; Carreno-Morelli, E.; Yang, F.; Raynova, S. Yield of Cyclic vs Heat-and-hold Induction Sintering on the Mechanical Behaviour of the Low-cost Ti-5Fe Alloy. *Mater. Sci. Eng. A* **2025**, *931*, 148235. [CrossRef]
19. Çivi, C.; Atik, E. The Effect of Inductive Sintering to Iron Based Powder Metal Parts. *J. Alloys Compd.* **2018**, *753*, 517–524. [CrossRef]
20. Kim, H.-C.; Kim, D.-K.; Woo, K.-D.; Ko, I.-Y.; Shon, I.-J. Consolidation of Binderless WC-TiC by High Frequency Induction Heating Sintering. *Int. J. Refract. Met. Hard Mater.* **2008**, *26*, 48–54. [CrossRef]
21. Plehanov, B.G. Experimental Results of Sintering Velocity of Powder Metallurgy Parts Sintered by High Frequency Induction Heating. *Porochkovaia Metall.* **1992**, *12*, 96–99.
22. Akechi, K.; Hara, Z. Increase of Sintering Rate of Titanium Powder During Cyclic Phase Transformation. *Powder Metall.* **1981**, *24*, 41–46. [CrossRef]
23. Kohara, S. Effect of Repeated Allotropic Transformation on Sintering of Iron Powder. *Metall. Trans. A* **1976**, *7*, 1239–1241. [CrossRef]
24. Zhang, X.; Zhou, J.; Lin, N.; Li, K.; Fu, K.; Huang, B.; He, Y. Effects of Ni Addition and Cyclic Sintering on Microstructure and Mechanical Properties of Coarse Grained WC-10Co Cemented Carbides. *Int. J. Refract. Met. Hard Mater.* **2016**, *57*, 64–69. [CrossRef]
25. Jiang, R.; Torresani, E.; Maximenko, A.; Wang, H.; Faulhaber, S.; Vecchio, K.; Olevsky, E.A. Cyclic Phase Transition-Assisted Spark Plasma Sintering of AlCoCrFeNi Complex Concentrated Alloys. *Metall. Mater. Trans. A* **2024**, *55*, 1111–1121. [CrossRef]
26. Morinaga, M.; Kato, M.; Kamikura, T.; Fukumoto, M.; Harada, I.; Kubo, K. Theoretical Design of β-type Titanium Alloys. In *Titanium '92, Science and Technology*; The Minerals, Metals & Materials Society (TMS): Pittsburgh, PA, USA, 1992; Volume 1, pp. 217–224.

27. Bolzoni, L.; Ruiz-Navas, E.; Neubauer, E.; Gordo, E. Mechanical Properties and Microstructural Evolution of Vacuum Hot-pressed Titanium and Ti-6Al-7Nb Alloy. *J. Mech. Behav. Biomed. Mater.* **2012**, *9*, 91–99. [CrossRef] [PubMed]
28. Ye, B.; Matsen, M.R.; Dunand, D.C. Enhanced Densification of Ti-6Al-4V Powders by Transformation-mismatch Plasticity. *Acta Mater.* **2010**, *58*, 3851–3859. [CrossRef]
29. O'Flynn, J.; Corbin, S. The Influence of Iron Powder Size on Pore Formation, Densification and Homogenization during Blended Elemental Sintering of Ti-2.5Fe. *J. Alloys Compd.* **2015**, *618*, 437–448. [CrossRef]
30. Fang, Z.Z.; Paramore, J.D.; Sun, P.; Chandran, K.S.R.; Zhang, Y.; Xia, Y.; Cao, F.; Koopman, M.; Free, M. Powder Metallurgy of Titanium—Past, Present, and Future. *Int. Mater. Rev.* **2018**, *63*, 407–459. [CrossRef]
31. Masikane, M.A.; Chikwanda, H.K.; Sigalas, I. A Comparative Study on the Sintering and Casting of a Blended Elemental Ti-6Al-4V Alloy. *Mater. Sci. Forum* **2015**, *828–829*, 421–426. [CrossRef]
32. German, R.M. Sintering Trajectories: Description on How Density, Surface Area, and Grain Size Change. *JOM* **2016**, *68*, 878–884. [CrossRef]
33. Bolzoni, L.; Esteban, P.; Ruiz-Navas, E.; Gordo, E. Mechanical Behaviour of Pressed and Sintered Titanium Alloys Obtained from Prealloyed and Blended Elemental Powders. *J. Mech. Behav. Biomed. Mater.* **2012**, *14*, 29–38. [CrossRef] [PubMed]
34. Guleryuz, H.; Cimenoglu, H. Oxidation of Ti-6Al-4V Alloy. *J. Alloys Compd.* **2009**, *472*, 241–246. [CrossRef]
35. Murray, J.L. *Phase Diagrams of Binary Titanium Alloys*; ASM International: Phoenix, AZ, USA, 1987; pp. 1–345.
36. Böhm, A.; Kieback, B. Investigation of Swelling Behaviour of Ti-Al Elemental Powder Mixtures during Reaction Sintering. *Z. Für Met.* **1998**, *89*, 90–95.
37. van Loo, F.; Rieck, G. Diffusion in the Titanium-aluminium System—I. Interdiffusion between Solid Al and Ti or Ti-Al Alloys. *Acta Metall.* **1973**, *21*, 61–71. [CrossRef]
38. Bolzoni, L.; Weissgaerber, T.; Kieback, B.; Ruiz-Navas, E.; Gordo, E. Mechanical Behaviour of Pressed and Sintered CP Ti and Ti-6Al-7Nb Alloy Obtained from Master Alloy Addition Powder. *J. Mech. Behav. Biomed. Mater.* **2013**, *20*, 149–161. [CrossRef] [PubMed]
39. Chen, Y.; Han, P.; Dehghan-Manshadi, A.; Kent, D.; Ehtemam-Haghighi, S.; Jowers, C.; Bermingham, M.; Li, T.; Cooper-White, J.; Dargusch, M.S. Sintering and Biocompatibility of Blended Elemental Ti-xNb Alloys. *J. Mech. Behav. Biomed. Mater.* **2020**, *104*, 103691. [CrossRef] [PubMed]
40. Kim, Y.; Lee, J.; Lee, B.; Ryu, H.J.; Hong, S.H. Dilatometric Analysis and Microstructural Investigation of the Sintering Mechanisms of Blended Elemental Ti-6Al-4V Powders. *Metall. Mater. Trans. A* **2016**, *47*, 4616–4624. [CrossRef]
41. Bolzoni, L.; Ruiz-Navas, E.; Gordo, E. Powder Metallurgy CP-Ti Performances: Hydride-dehydride vs. sponge. *Mater. Des.* **2014**, *60*, 226–232. [CrossRef]
42. German, R.M. Titanium Sintering Science: A Review of Atomic Events during Densification. *Int. J. Refract. Met. Hard Mater.* **2020**, *89*, 105214. [CrossRef]
43. Yan, M.; Xu, W.; Dargusch, M.S.; Tang, H.P.; Brandt, M.; Qian, M. Review of Effect of Oxygen on Room Temperature Ductility of Titanium and Titanium Alloys. *Powder Metall.* **2014**, *57*, 251–257. [CrossRef]
44. Poulain, R.; Amann, F.; Deya, J.; Bourgon, J.; Delannoy, S.; Prima, F. Short-time Heat Treatments in Oxygen Strengthened Ti-Zr α Titanium Alloys: A Simple Approach for Optimized Strength-ductility Trade-off. *Mater. Lett.* **2022**, *317*, 132114. [CrossRef]
45. Kumar, P.; Chandran, K.S.R. Strength-Ductility Property Maps of Powder Metallurgy (PM) Ti-6Al-4V Alloy: A Critical Review of Processing-Structure-Property Relationships. *Metall. Mater. Trans. A* **2017**, *48*, 2301–2319. [CrossRef]
46. Sun, J.; Pan, Y.; Liu, Y.; Kuang, F.; Wu, X.; Cao, P.; Lu, X. The Designed High-performance PM Ti-6Al-4V Alloy via Two-step Pressureless Sintering. *J. Alloys Compd.* **2024**, *976*, 173324. [CrossRef]
47. Robertson, I.; Schaffer, G. Some Effects of Particle Size on the Sintering of Titanium and a Master Sintering Curve Model. *Metall. Mater. Trans. A* **2009**, *40*, 1968–1979. [CrossRef]

Disclaimer/Publisher's Note: The statements, opinions and data contained in all publications are solely those of the individual author(s) and contributor(s) and not of MDPI and/or the editor(s). MDPI and/or the editor(s) disclaim responsibility for any injury to people or property resulting from any ideas, methods, instructions or products referred to in the content.